Optics & Laser Technology 134 (2021) 106639

Contents lists available at ScienceDirect

Optics and Laser Technology

journal homepage: www.elsevier.com/locate/optlastec

Full length article

Laser polishing for improving fatigue performance of additive manufactured Ti-6Al-4V parts

Seungjong Lee [a,b], Zabihollah Ahmadi [c], Jonathan W. Pegues [d], Masoud Mahjouri-Samani [b,c,*], Nima Shamsaei [a,b,*]

[a] Department of Mechanical Engineering, Auburn University, Auburn, AL 36849, USA
[b] National Center for Additive Manufacturing Excellence (NCAME), Auburn University, Auburn, AL 36849, USA
[c] Department of Electrical and Computer Engineering, Auburn University, Auburn, AL 36849, USA
[d] Material, Physical, and Chemical Sciences Center, Sandia National Laboratories, Albuquerque, NM 87185, USA

ARTICLE INFO

Keywords:
Fatigue
Microstructure
Surface roughness
Surface laser processing
Laser beam powder bed fusion

ABSTRACT

Additive manufacturing of metallic materials is rapidly growing due to the possibility of constructing customized products with complex geometries. The mechanical properties of additively manufactured parts often show inconsistent performance when compared against their wrought counterparts. The fatigue performance is often severely undermined by the presence of process-induced defects and in particular surface roughness, hence requiring a post-processing method to treat the surface of additively manufactured metallic parts. In this study, laser polishing is presented as a fast, efficient, and precise approach for post-processing of additively manufactured parts. The alpha-beta titanium alloy (Ti-6Al-4V) specimens were fabricated by laser beam powder bed fusion (LB-PBF) method and subsequently surface-treated by a continuous wave fiber laser in a controlled environment. A comprehensive study was performed to determine the optimum process parameters of laser polishing. Results indicated that the high cycle fatigue lives of the laser polished parts were somewhat longer than the as-built specimens due to reduced surface roughness. Inevitable residual stresses were introduced by laser polishing; however, it was successfully relaxed by a secondary stress relief process. Moreover, the laser polished and secondary stress relieved specimens had improved fatigue strengths at all life regimes.

1. Introduction

The additive manufacturing (AM) of metallic materials has been an area of increasing interest both in academia and industry because of its remarkable advantages in design versatility and fabrication of complex geometries [1–4]. Near-net-shape parts are created via computer-aided design software, and completed design files are adopted by the AM machine. Fabricating separate parts and assembling each component can be eliminated by AM, hence saving tremendous time and materials. Additionally, the layer-by-layer process of AM makes it possible to construct complicated geometries such as lattice structures and internal features not possible through subtractive methods. Several applications which have been identified as attractive for AM include, for example, fabricating bone implants for the biomedical industry [5], printing lightweight components for the aerospace industry [6], as well as fabricating or repairing complex components such as steam and turbo-engine blades/cases [7].

Titanium is acknowledged as an attractive material for both traditional manufacturing and AM because of its high strength to weight ratio compared to other materials [8–12]. Ti-6Al-4V is one of the most widely-used alpha-beta titanium alloys in the aerospace and biomedical industries. Traditionally manufactured Ti-6Al-4V parts, however, require extensive machining or forging procedures to shape the final design, which are often associated with high material waste, long lead times, and unattractive costs [13,14]. Therefore, AM of Ti-6Al-4V components has received considerable attention since it enables the near-net-shape fabrication of parts with minimal machining requirements. Post-

Abbreviations: AB, As-built; AM, Additive manufacturing/Additive manufactured; EBM, Electron beam melting; EBSD, Electron backscatter diffraction; FIB, Focused ion beam; HCF, High cycle fatigue; ICF, Intermediate cycle fatigue; LB-PBF, Laser beam powder bed fusion; LCF, Low cycle fatigue; LP, Laser polishing/polished; LPSR, Laser polished and secondary stress relieved; M/P, Machined and polished; SEM, Scanning electron microscope/microscopy; SR, Surface roughness; TEM, Transmission electron microscope/microscopy.

* Corresponding authors at: National Center for Additive Manufacturing Excellence (NCAME), Auburn University, Auburn, AL 36849, USA.
E-mail addresses: mahjouri@auburn.edu (M. Mahjouri-Samani), shamsaei@auburn.edu (N. Shamsaei).

https://doi.org/10.1016/j.optlastec.2020.106639
Received 30 June 2020; Received in revised form 4 September 2020; Accepted 28 September 2020
Available online 14 October 2020

Nomenclature

α	Alpha
α'	Alpha prime
β	Beta
ε_a	Strain amplitude
$2N_f$	Reversals to failure
R	Stress-ratio
R_a	Arithmetical mean height of the profiled line
R_v	Maximum valley height of the profiled line
R_z	Maximum peak-to-valley height of the profiled line
S_a	Arithmetical mean height of the profiled surface
S_v	Maximum valley height of the profiled surface
S_z	Maximum peak-to-valley height of the profiled surface
σ_a	Stress amplitude

processing is often still required, however, in order to reduce the surface roughness (SR) of as-built parts despite AM providing net shape [15].

Among various mechanical properties, the fatigue strength is considered as a major concern since a common mode of mechanical failure is caused by cyclic loading. In terms of fatigue behavior, the primary vulnerability of AM parts is SR. Previous studies confirmed that the step effect resulting from the layer-by-layer fabrication process tremendously could reduce the fatigue strength of AM parts [16–18]. The AM process also results in partially melted powder particles on the part's surface [19,20]. Therefore, the partially-melted powder particles induce topographical features that have sharp valley points along the surface, which act as micro-notches and induce early life fatigue crack initiation, adversely affecting the fatigue strength [21].

In order to moderate the SR of AM parts, various surface post-processing methods have been developed or imported from the conventional manufacturing community [22]. The most widely utilized surface improvement method which fully removes SR is the physical machining process including lathing, milling, grinding, etc. However, the machining process not only wastes the material but also can introduce deformation into the part. Additionally, AM is most effective when you fabricate parts with complex geometries which are difficult, if not impossible, to remove SR by machining. Therefore, additional methods for surface processing of AM components are critical and must be investigated. As a potential post-processing method, laser polishing (LP) can remelt partially melted particles on the surface, reconstruct surface topography, and alter the surface microstructure of AM parts without wasting materials or destroying the original shape. The interaction of a laser beam, having a suitable power density, with the surface of the AM parts can rapidly melt the surface structures. The temperature of the melted area drops quickly as the laser moves forward, resulting in the rapid solidification of the molten pool similar to the LB-PBF process [23–25] without significant material loss. Therefore, the study of the LP technique has been recently growing [26,27].

LP has been studied for both conventionally manufactured and AM parts using various types of lasers. Guo et al. [28] successfully decreased SR of machined ASSAB DF2 cold work (AISI O1) tool steel from 0.4 μm to 0.12 μm using microsecond Nd: YAG laser. Giorleo et al. [29] also showed a reduced SR in titanium sheets from 0.58 μm to 0.42 μm utilizing Nd: YVO4 laser. In the AM community, especially, the effects of LP on microstructure and fatigue strength of AM parts have been partially investigated. Tian et al. [30] investigated the effect of LP on the microstructure of electron beam melted Ti-6Al-4V components; however, no fatigue testing was performed in this study. Kahlin et al. [15] and Liang et al. [31] conducted fatigue testing after LP to observe improvements in fatigue strength of LB-PBF Ti-6Al-4V. Although in these studies, the SR was reduced by LP, they did not observe significant increases in fatigue strength as compared to the parts in their as-built surface condition.

Table 1
The chemical composition of Ti-6Al-4V powder produced by Carpenter Additive.

Element	Al	C	H	Fe	N	O	Ti	V
Wt. %	6.2	0.01	0.002	0.09	0.01	0.09	Bal	4.0

This study incorporates a post-process LP to LB-PBF Ti-6Al-4V fatigue specimens targeting lower SR and improved fatigue resistance compared to as-built surface condition, and hopefully comparable to machined/polished (M/P) surface condition. The effect of stress relief is also investigated to decouple any thermal history effects introduced by remelting the surface during the LP. The measured effective thickness of LP zone was verified to sufficiently cover the maximum range of as-built SR and cancel out the defects close to the surface. Fractography analysis confirmed that cracks of specimens after LP were not initiated from the surface but the defect under the laser treated region. Moreover, changes in microstructural characteristics are discussed.

2. Materials and methods

The specimens were fabricated by a laser beam powder bed fusion (LB-PBF) AM machine (EOS M290) using grade 23 Ti-6Al-4V powder produced by Carpenter Additive. The chemical composition of the powder is shown in Table 1. The AM process parameters were the default EOS recommended parameters for Ti-6Al-4V (i.e., laser power of 280 W, laser scan speed of 1200 mm/s, hatching distance of 0.14 mm, and layer thickness of 30 μm). The fatigue specimen geometry was designed in accordance with the study conducted by Carrion et al [32], with the dimensions of the specimen described in Fig. 1. The build orientation was perpendicular to the substrate; thus, side support structures were fabricated to prevent failure during the recoating process. In addition, an increased interlayer time interval was incorporated into the process by adding a ghost specimen that received 0 W power to improve the cooling of the specimens.

Fig. 2 describes the details of the build plate that included specimens, side support structures, and the ghost specimen. The building process was conducted under an argon atmosphere (the differential pressure of 0.6 mbar) and the build plate temperature of 35 °C. The specimens were removed from the substrate by band saw carefully protecting the specimens from inadvertent damage to the surfaces during the removal procedure. After removal from the substrate, the stress relief process was conducted for every specimen to release the residual stresses. The stress relief was conducted inside a tube furnace in an argon environment at 700 °C for an hour, followed by furnace-cooling to room temperature. In this study, the specimen before LP is referred to as as-built (AB) and after LP as laser polished (LP). In addition, a group of LP specimens were stress relieved again to remove any potential residual stresses as a result of LP; these specimens are referred to as laser polished and stress relieved (LPSR).

A CW fiber laser (SPI RedPower, 1064 nm wavelength) was utilized for the LP of LB-PBF Ti-6Al-4V parts in this study. This fiber laser was coupled to a galvo scanner with an F-theta lens that provides about 15 μm focal point on the surface of the specimens. A control software (Laser Studio Professional) was utilized to design laser scanning patterns and adjust the process parameters, including laser power, scanning speed, and hatching distance. Under the galvo scanner, a rotary axis and a costume-built environmental chamber were installed, as shown in Fig. 3. The specimens were gripped on the rotary axis, and rotation was programmed to achieve the desired hatch spacing between laser tracks. The custom-built chamber maintained an inert argon environment during the LP process to avoid surface oxidation. The argon pressure and flow rate for LP were atmospheric pressure and 30 L per minute, respectively. Various laser powers (ranging from 10 to 180 W) and scanning speeds (ranging from 10 to 400 mm/s) were tried to find applicable process parameters. The laser power of 120 W, scanning speed of 100 mm/s, and hatching space of 10 μm were selected as the appropriate laser process

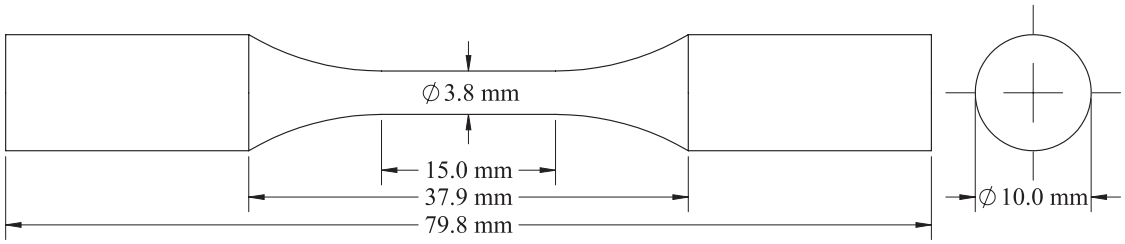

Fig. 1. Dimensions and geometry of LB-PBF Ti-6Al-4V fatigue specimens used in this study.

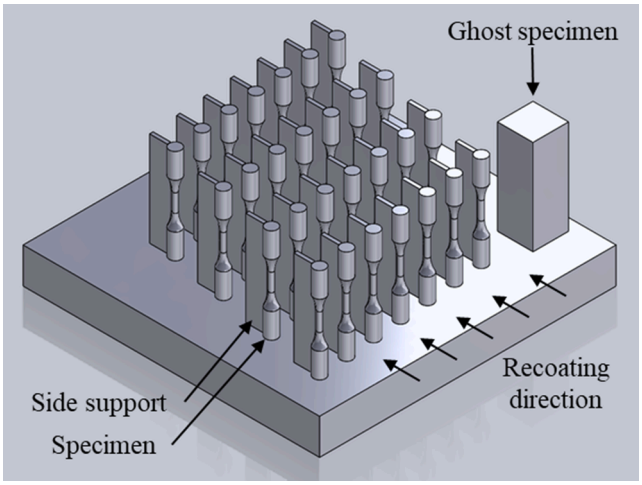

Fig. 2. The schematic of the fabrication layout. Side supports were perpendicular to the direction of the recoating process. The ghost specimen with 0 W laser power was located at the corner to increase the time interval between each layer.

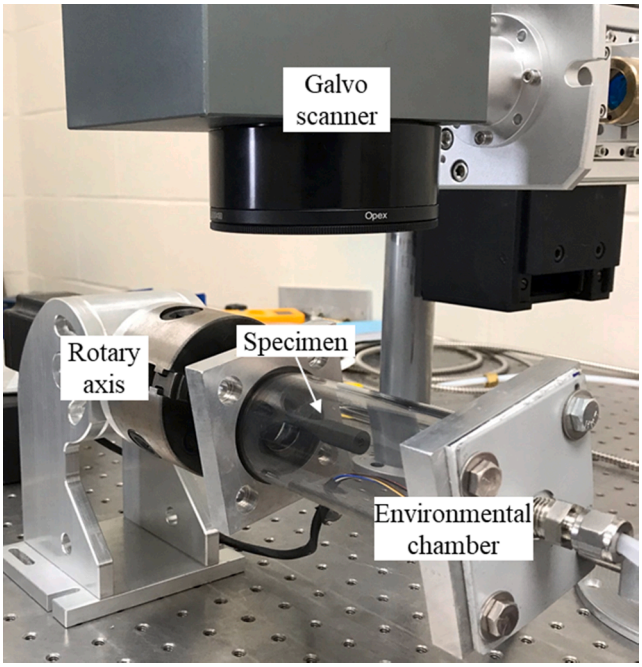

Fig. 3. Laser polishing (LP) setup. A control software was used to set the galvo scanner and laser process parameters. Specimens were held by a rotary axis inside an environmental chamber for laser processing in an inert argon environment.

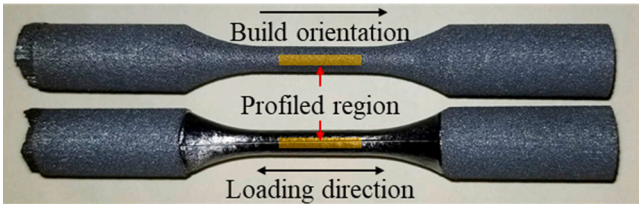

Fig. 4. An image showing the entire specimens with AB (top) and LP (bottom) surfaces along with the build orientation and the loading direction. LP was done by scanning the laser beam parallel to the loading direction. The surface roughness profiled regions are shown here by yellow color. (For interpretation of the references to color in this figure legend, the reader is referred to the web version of this article.)

parameters based on the resulting SR, near-surface defect distributions, and microstructures.

The surface of the gage section was observed by a 3D optical microscope (Keyence VHX-6000) to investigate surface topography. To compare the surface conditions, SR parameters before and after LP were measured. The profiled surface directions were parallel to the build direction, as shown in Fig. 4, since this direction contains the layer-wise surface roughness, which has been shown to promote the highest roughness for AM parts [16,18]. In this study, a 3 mm section along the build orientation was profiled. The longer profile was needed to provide more precise SR values, and the 3D stitching function in the microscope software was used to capture large areas. The 3D images were obtained at 500× magnification to increase the relative accuracy of the point height data. In this study, five-line roughness profiles, as well as area roughness were obtained and analyzed.

The microstructures of the specimens were investigated by both a 3D optical microscope and a scanning electron microscope (SEM, Zeiss Crossbeam 550). In order to measure the thickness of the LP layer using digital microscopy, the radial cross-sections at the gage of the specimens after LP were cut, polished, and chemically etched using Kroll's etchant for approximately 20 s. For the microstructure analysis, polished samples without etching were investigated by the SEM. In order to check the microstructure after LP, the region influenced by LP was milled using a focused ion beam (FIB) and observed by SEM. All measurements were conducted under the same configurations for consistent comparison of microstructures (i.e., 7,000× magnification with 5 kV for the inner part and 18,000× magnification with 2 kV for the part close to the surface after FIB).

The fatigue testing was conducted on a servo-hydraulic load frame (MTS 810) with 100 kN capacity. Carrion et al. studied the fatigue behavior of M/P LB-PBF Ti-6Al-4V specimens that were fabricated by using similar material and design criteria [30]. This study replicated the test setup, fully reversed ($R = -1$) strain-controlled fatigue tests at similar strain levels, in order to utilize the M/P data provided in [30] as a baseline in this study. An extensometer was installed on the gage section to measure and control strain amplitude (a sinusoidal waveform) during testing. Four different strain amplitude/frequencies combinations were utilized to maintain similar average cyclic strain rates for each strain level. Each strain level included 2–4 tests.

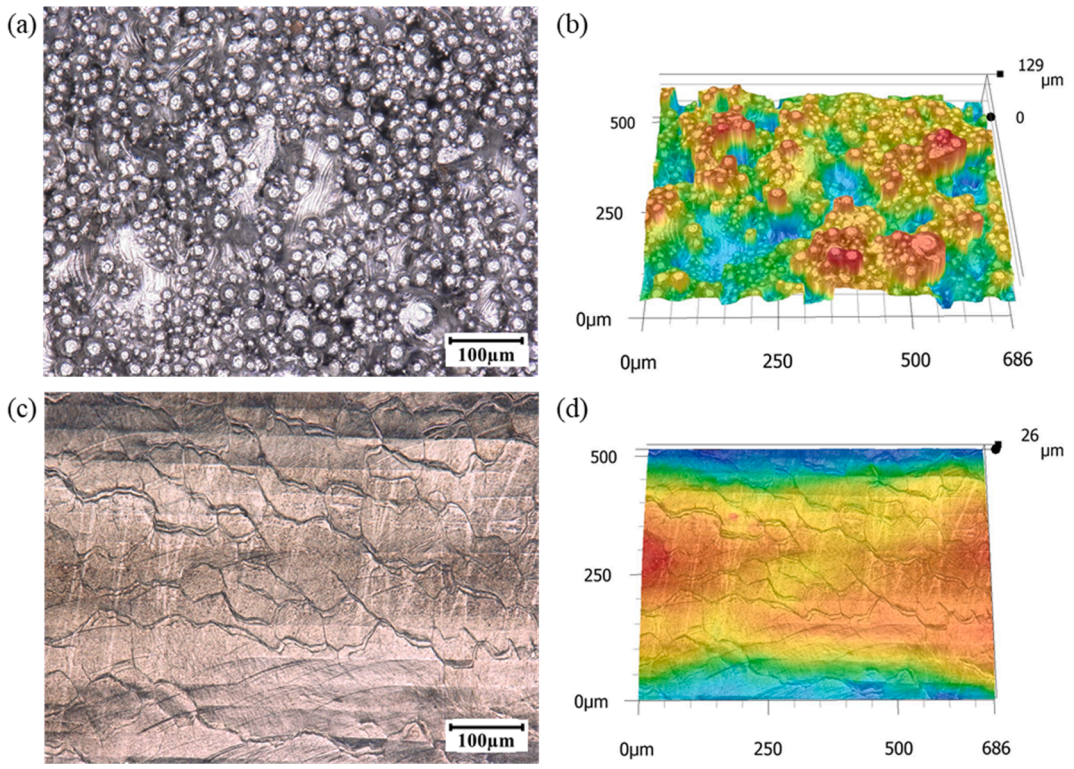

Fig. 5. Surface conditions before and after the LP: (a) optical image of an AB surface and (b) its 3D analyzed AB surface with color map and scale indicating the large surface roughness. (c) Optical image of a LP surface and its (d) 3D analyzed LP surface.

Table 2
The average and standard deviation values of SR parameters for both AB and LP surface conditions based on ISO 4287:1997 surface texture: profile method [31]. The unit is in μm.

	R_a	R_z	R_v	S_a	S_z	S_v
AB	14.23 (3.28)	90.58 (19.72)	43.26 (9.53)	15.53 (2.30)	134.97 (20.18)	67.56 (13.22)
LP	6.01 (1.63)	28.02 (5.43)	13.30 (3.25)	7.92 (1.49)	57.15 (11.33)	32.90 (10.45)
% Reduction	57.8	69.1	69.3	49.0	57.7	51.3

For the HCF regime ($\varepsilon_a = 0.002$ mm/mm), tests were paused after reaching 10^6 cycles to remove the extensometer. Tests were then continued under force-controlled loading with the stress amplitude being estimated from the stable hysteresis loop during strain-controlled loading. The tests were continued until failure, while the tests reaching 10^7 reversals being suspended and considered as run-outs. The fracture surfaces were inspected by digital microscopy. First, the entire fracture surface was observed using 3D stitching at 300× to study the macroscopic characteristics of the cracks. The crack initiation region was observed at higher magnification in order to elucidate the crack initiation differences between the surface conditions before and after LP.

3. Experimental results and discussion

3.1. Surface improvements

The LP appropriately remelted the powder particles and reconstructed the surface topography. AB surface conditions showed an extremely rough surface with randomly located peaks and valleys, as described in Fig. 5(a) and (b). In contrast, after LP, a smooth surface as shown in Fig. 5(c) and (d) was achieved. The averages and standard deviations of investigated line roughness and area roughness values based on ISO 4287:1997 [33] are listed in Table 2. In order to improve statistical reliability, 30 profiled lines were considered (6 specimens, 5 lines for each specimen). The LP successfully decreased all SR values by approximately 60–70%. The most commonly used SR values, R_a and S_a showed a ~ 50% reduction. Among the investigated SR parameters, interestingly, the maximum valley depth of the profiled line (R_v) showed the most reduction (~69%) in average value.

Before and after LP, the measured cross-sectional areas were changed even though LP did not waste any material during the process. The average cross-sectional area of specimens with an as-built surface was 10.28 mm^2; on the other hand, the area was decreased to 9.75 mm^2 after LP. Pegues et al. [34] claimed that the measured cross-sectional area and the load-bearing area is different due to unnecessarily measured SR. When the maximum peak-to-valley depth of the profiled line (R_z) was utilized as a correction value, the cross-sectional area was decreased from 10.28 mm^2 to 9.58 mm^2. Therefore, a disparity of the cross-sectional area between AB and LP surfaces is reduced from 5.4% to 1.7%. This observation confirms that the load-bearing area should be considered with the effect of SR, especially when designing the small components.

The LP specimens contained some marks on the surface which were similar in appearance to grain boundaries, as shown in Fig. 5(c). According to studies regarding laser welding, solidification cracks can develop by LP through non-optimal process parameters [35,36] and these marks were different from solidification cracks observed for other scanning parameters. Tian et al. [30] claimed that these marks in Fig. 5 (c) are not solidification cracks but grain boundary groovings caused by surface tension. In order to characterize these marks, the LP surfaces

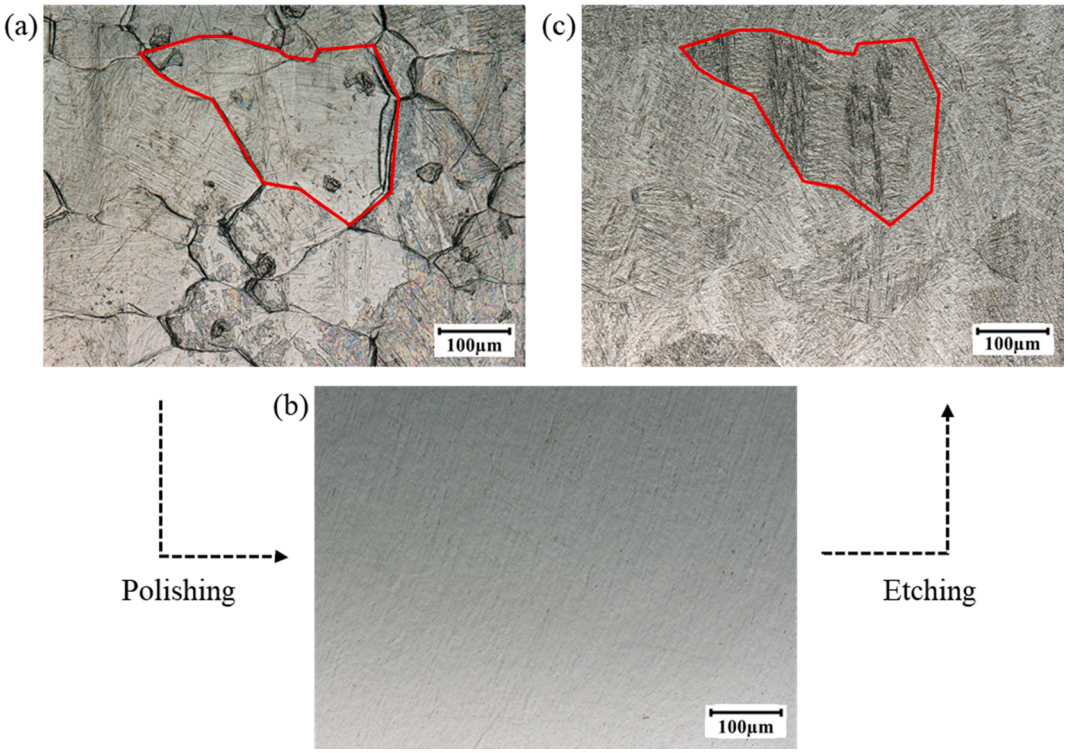

Fig. 6. Surface characterization of an LP specimen. Optical microscopic images of (a) LP surface, (b) mechanically polished surface after etching (~1 μm), and (c) chemically etched surface after polishing. The prior β grain boundary is shown in line in (a) and (c).

were polished then etched to reveal the general microstructure, as shown in Fig. 6. The (a) LP surface condition was observed first, (b) mechanically polished, and (c) chemically etched surface textures were investigated, as shown in Fig. 6. The same location was measured repeatedly for each condition and showed these features indicated by red lines aligned with the prior β grain boundaries. It verified that these marks are grain boundary groovings and should not necessarily be considered as initial cracks.

Surface topography analyses using pixel-height data of 3D scanned profiles before and after LP were conducted by Matlab, as described in Fig. 7. The figures with colormap on the left side described 3D shapes on the surface and the plots on the right detail the profiles of the corresponding sectioning plane from the left image. According to Fig. 7(a) for AB surface and (c) LP surface, LP guaranteed both numerical and topographical improvements in SR. The depth of SR was significantly reduced after LP from ~ 80 μm to ~ 15 μm as described in Fig. 7(b) and (d) 2D profiles. Some sharp notches were observed after LP as shown in Fig. 7(c) and (d). However, these sharp notches were not always critical to fatigue resistance since the combined depth and sharpness considered together were much lower than what was observed for the AB surfaces.

SR acts as micro-notches on the surface of the specimens, introducing stress concentrators at the valleys. The maximum valley height (R_v), potentially represents the critical depth for crack initiation in terms of fatigue failure [37]. The LP reduced R_v the most among SR parameters listed in Table 2. Surface polishing capable of reducing S_v may be preferable to other post-processing such as sandblasting, chemical polishing, and electropolishing which do not affect S_v to the same extent as LP [38]. According to Pegues et al. [21], both SR values and geometrical shapes of notches should be considered to understand the true impact of the SR on fatigue resistance. The notches on the AB surface have deep valleys with very small radii (deep, sharp notches) as shown in Fig. 7(a) and (b), while LP surfaces provide shallower valleys with larger radii (shallow, blunt notches) as described in Fig. 7(e) and (f). As such, the expected stress concentrations for a deep and sharp surface feature (i.e. AB surfaces) would be much greater than a shallow blunt surface feature (i.e. LP surfaces), potentially leading to lower fatigue strengths as observed for specimens in AB surface condition.

The LP partially remelted and resolidified the surface, and the reconstructed area was confined to the laser path (melt pool generated by LP). Therefore, LP parameters did not result in complete removal of the surface undulations which can be much larger than the melt pool size, but rather reduced the depth and sharpness of the valleys, which are critical to fatigue resistance. Therefore, significant unevenness (i.e. high surface roughness in electron beam melting (EBM) caused by larger layer thickness [39,40]) cannot be fully reconstructed. Even though LB-PBF utilizes smaller layer thickness, LB-PBF specimens after LP still showed surface undulations. For example, Fig. 7(e) and (f) show the LP surface profile which is smoother than AB surface, shown in Fig. 7(a) and (b). However, it has more gradual undulations on the surface compared to Fig. 7(c) and (d), even though the process parameters were the same. Such variations seen on the surface of LP specimens may be caused by the nature of LB-PBF process; including but not limited to, powder characteristics, powder spreading by a recoater blade, gas flow/direction, and spattered particles. In order to completely remove the gradual surface undulations, more in-depth studies are needed to fully optimize the processes parameters, including multiple pass LP, hatching distance, power, and scanning speed.

3.2. Fatigue behavior and fractography

The strain-controlled fatigue testing results of LB-PBF Ti-6Al-4V including surface conditions, frequencies, strain amplitudes, stress amplitudes, and reversals to failure are listed in Table 3. As explained in Section 2, the baseline M/P specimens' results were taken from the previous study, which had the same design criteria [32]. The strain-life fatigue plot, presented in Fig. 8, was generated from the data tabulated

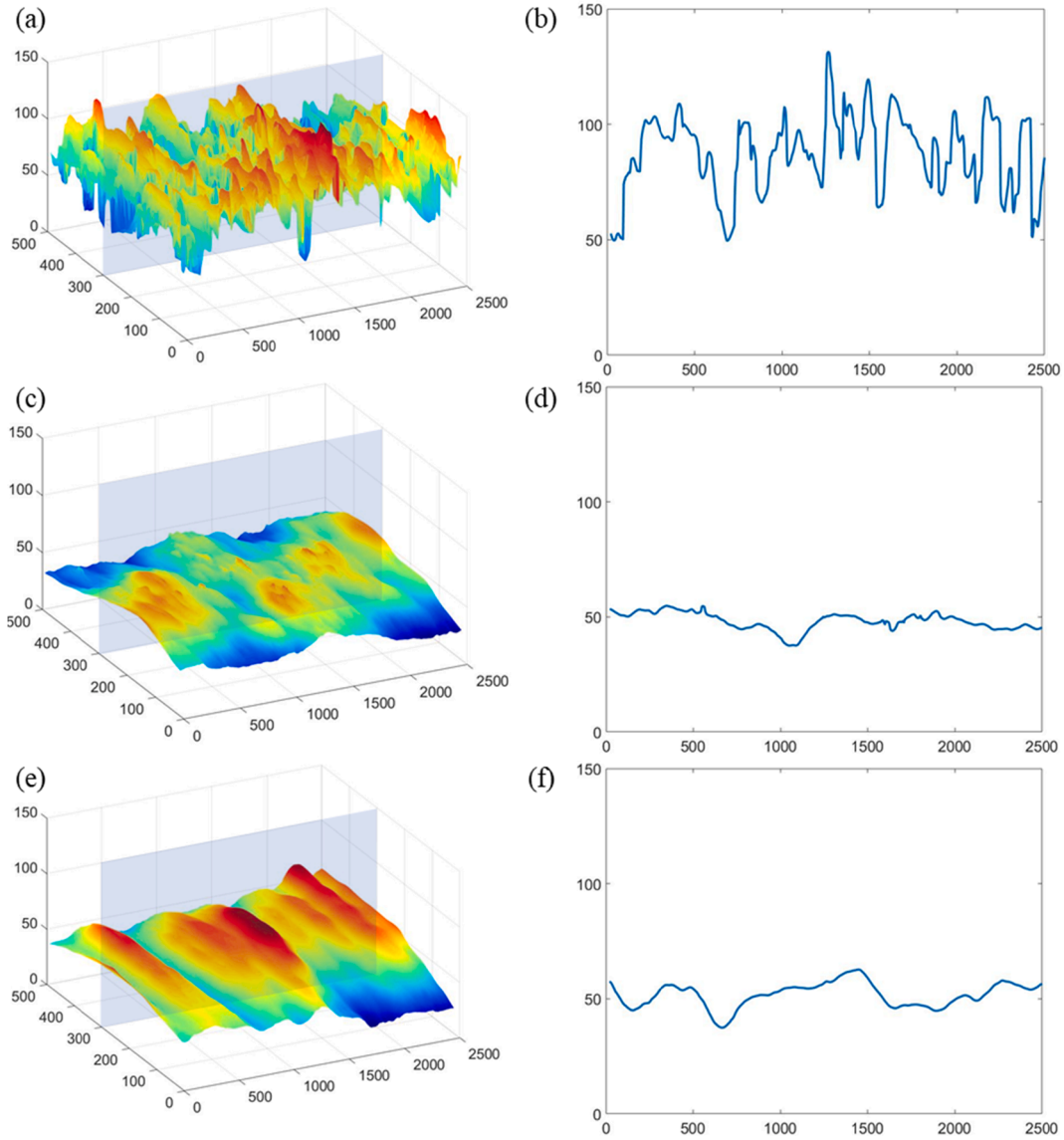

Fig. 7. 3D and 2D surface topology images for each surface condition generated by pixel-height data using Matlab. 2D images show the height of the profiled area (*shaded area*) from the 3D color maps including (a) 3D AB surface, (b) 2D AB surface of (a), (c) 3D LP surface, (d) 2D LP surface of (c), (e) 3D LP surface which has surface undulation regions, and (f) 2D LP surface of (e). The unit is in μm. (For interpretation of the references to colour in this figure legend, the reader is referred to the web version of this article.)

in Table 3. Four different symbols represent each surface and stress relief condition: green triangles for specimens with as-built surface condition (AB); blue diamonds for specimens with laser polished surface condition (LP); red circles for specimens with laser polished surface condition and secondary stress relief (LPSR); black squares for machined/polished specimens as the baseline (M/P). It should be reminded here that all of these specimens had gone through stress relieving the thermal cycle after removal from the built plate and before testing or LP.

The fatigue strength of LP specimens was improved at lower strain levels (i.e. intermediate cycle fatigue (ICF) and high cycle fatigue (HCF)) as shown in Fig. 8 compared to the AB specimens. The fatigue lives of LP specimens in the HCF regime were at least one order of magnitude longer than AB specimens. Nevertheless, LP specimens had clearly lower fatigue strengths than the AB specimens at higher strain levels (i.e. low cycle fatigue (LCF)), which may be related to possible residual stresses generated on the surface of the LP specimens due to the LP process. LP can generate undesirable residual stresses due to a compressive plastic misfit related to the irregular thermal stresses such as localized heat volume expansion caused by a small irradiated area [30]. Even though LP generated inevitable residual stresses, the effect of SR on fatigue strength in the HCF regime can be more significant than the generated residual stresses. Therefore, LP specimens still exhibited longer fatigue lives than AB specimens in the ICF and HCF regimes, even when secondary stress relief is not performed. In contrast, there is less effect of SR in LCF due to the significant plastic deformation in the material [41]. As a result, the influence of the high plastic strain amplitudes may collaborate with tensile residual stresses to produce more detrimental effects. Essentially, the influence of the residual stress may be greater than the effect of surface roughness in the LCF regime.

LPSR specimens showed greater fatigue strengths than both AB and LP specimens. Moreover, one LPSR specimen tested under 0.004 mm/mm strain amplitude reached 10^7 reversals (run-out), which is comparable to M/P specimens. Fatigue testing results implied that residual stresses were successfully decreased by a stress relief process (one hour at 700°C under argon atmosphere) since it was the only difference between LP and LPSR specimens. Tian et al. [30] also demonstrated that

Table 3
Summary of fully reversed (R = −1) strain-controlled fatigue testing results: surface conditions, frequencies, strain amplitudes, stress amplitudes, and number of reversals to failure.

Test ID	Frequency (Hz)	ε_a (mm/mm)	σ_a (MPa)	$2N_f$ (Reversals)
AB #1	2	0.005	579	17,008
AB #2	2	0.005	563	17,798
AB #3	3	0.004	455	33,458
AB #4	3	0.004	474	37,284
AB #5	4	0.003	347	110,374
AB #6	4	0.003	341	121,312
AB #7	5	0.002	234	278,230
AB #8	5	0.002	235	380,546
LP #1	2	0.005	612	8146
LP #2	2	0.005	580	8438
LP #3	2	0.005	615	9438
LP #4	2	0.005	603	10,756
LP #5	3	0.004	465	70,718
LP #6	3	0.004	466	91,302
LP #7	4	0.003	364	1,306,726
LP #8	4	0.003	360	2,938,424
LP #9	5	0.002	242	>10000000
LP #10	5	0.002	239	>10000000
LPSR #1	2	0.005	617	21,998
LPSR #2	2	0.005	619	26,684
LPSR #3	2	0.005	611	47,496
LPSR #4	2	0.005	617	58,728
LPSR #5	3	0.004	488	146,864
LPSR #6	3	0.004	489	2,771,378
LPSR #7	3	0.004	498	>10000000

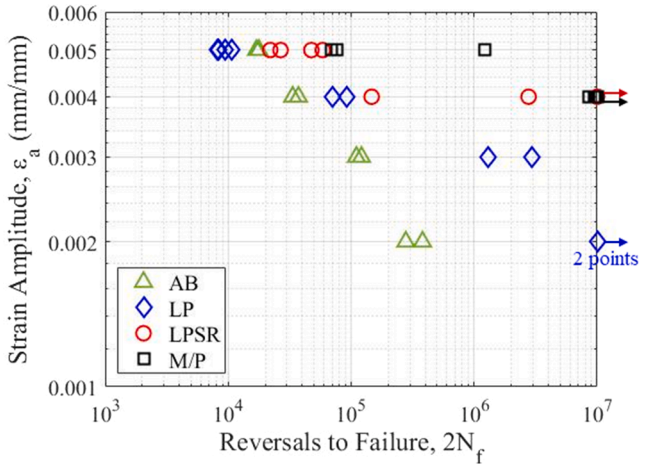

Fig. 8. The strain-life fatigue data for LB-PBF specimens with different surface and stress relief conditions. Arrows indicate run-out tests and their numbers (each arrow for one run-out test).

the conventional stress relief process (4 h at 750°C under vacuum condition) relaxed tensile residual stresses to near zero in EBM Ti-6Al-4V parts. However, multiple tests at 0.004 mm/mm strain amplitude failed before reaching 10^7 reversals with one test failing before 10^5 cycles. While the disparity between the shortest and longest observed fatigue lives at this strain amplitude is ~ 2 orders of magnitude, the improvement in fatigue strengths, compared to AB and LP specimens, is considerable. In general, the improvement in fatigue resistance, in ICF and HCF regimes, follows the hierarchy of AB < LP < LPSR < M/P and indicating that LP can be a viable means to improve the fatigue resistance of AM parts by reducing their SR.

Final fracture surfaces of AB and LP specimens confirmed that the crack initiations of each surface condition are distinct, as shown in Fig. 9. Every AB specimen generated multiple crack initiation sites on the surface, regardless of strain amplitude (Fig. 9(a)). On the other hand, the LP specimen showed a single dominant crack initiation at a defect located in ~ 300 μm from the surface under 0.003 mm/mm strain amplitude (Fig. 9(b)). This observation again indicated that LP can favorably reconstruct SR and heal defects close to the surface. More explanation regarding the healing defects close to the surface will be followed in Section 3.3.

LP did not always result in shifting the crack initiation from the surface to internal defects. An LP specimen tested with 0.004 mm/mm strain amplitude initiated a single crack on the surface (Fig. 9(c)), and another specimen tested with 0.005 mm/mm strain amplitude had multiple cracks initiating on the surface (Fig. 9(d)). Surface crack initiations after LP were sometimes occurred by either the error during LP procedure such as unstable rotation (Fig. 9(d)) and mismatch of the last laser scan path (Fig. 9(c)) or inevitable tensile residual stresses on the surface explained above. In order to utilize LP as the surface post-processing method, more precise procedures and secondary stress relief process are needed.

It is interesting to note that the LPSR fatigue lives showed larger scatter than AB and LP specimens under both 0.004 and 0.005 mm/mm strain amplitudes. This may reflect cracks being initiated both at the surface and internally at defects which are often observed for M/P conditions. By examining crack initiations in LPSR specimens through fractographic images, the specimen which has lower fatigue lives has multiple crack initiations on the surface. The test with longer fatigue lives showed cracks initiating at defects internal to the surface, which correspond to lower stress intensity factors, and consequently longer fatigue lives [42]. Despite the variation in fatigue lives, these observations suggest that LP tends to shift crack initiation from surface roughness to volumetric defects and is an effective surface treatment process that can provide many benefits not obtainable through other surface treatment procedures. Similar to some other surface treatment methods such as shot-peening and laser-peening, the first benefit of the LP is the reduced material waste; the surface is restructured rather than removed [15]. Additionally, the remelting process has the potential to remove near-surface defects within the laser influenced region. Finally, LP can be applied to parts with more complex geometries, for which surface machining may not be a viable option.

3.3. Microstructure characterization

Many studies have shown that SR acts as a dominant factor in the HCF regime using the fatigue curve trends between AB and M/P surface conditions [1,10–12,39,42–45]. Even in the LCF regime, M/P specimens have better fatigue strength than AB specimens. Interestingly, the LP provided distinct results as shown in Fig. 8. LP specimens without stress relief showed longer lives than AB specimens in the ICF and HCF regimes. However, they had deficient fatigue strength compare to the AB specimens in the LCF regime. The difference between LP and M/P specimens may come from the fact that LP not only reduced SR but also changed microstructures.

The thickness of the region influenced by LP was examined to investigate the microstructure of the laser-treated regions and to confirm whether or not the LP process completely envelops the entire surface structures. The longitudinal-section and radial cross-section of the LP specimens were polished and etched, as shown in Fig. 10. The images with low magnification as shown in Fig. 10(b) and (d) confirmed that LP changed the microstructure under the surface. The columnar grains normal to the cross-sectional area (parallel to build direction) were located in the middle of the part (see Fig. 10(b)) and the laser-treated region showed analogous columnar grains perpendicular to the build direction (see Fig. 10(d)). According to the high magnification images, Fig. 10(c) and (e), the average thickness of the laser-treated region is about 246 μm. Tian et al. [30] also measured both the remelted layer and heat-affected zone, and the values were roughly 180 μm and 250 μm which the latter is similar to our study.

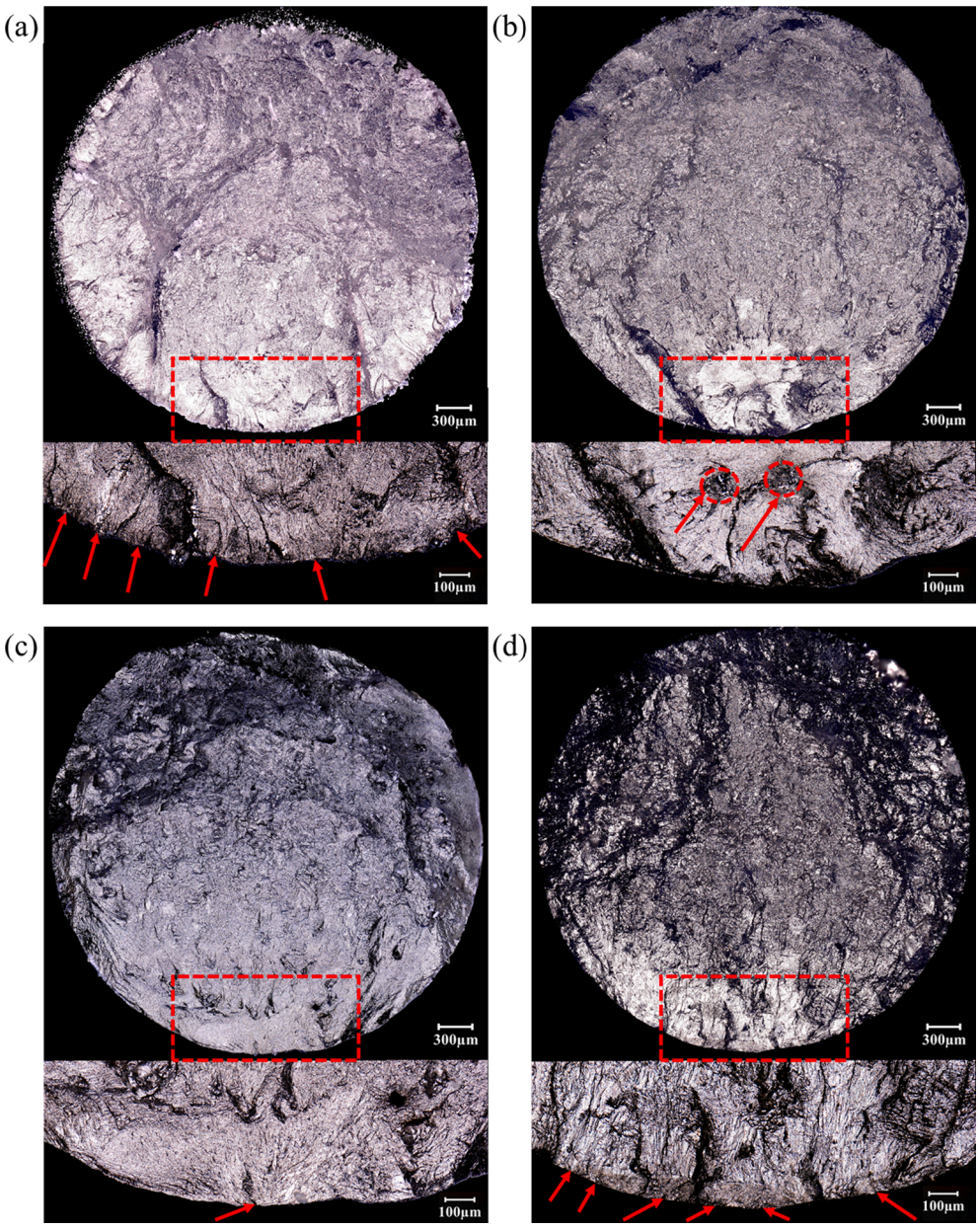

Fig. 9. Fracture surfaces showing various crack initiating phenomena for each surface condition: (a) AB specimen under 0.004 mm/mm strain amplitude (AB #3) having multiple crack initiations on the surface, (b) LP specimen under 0.003 mm/mm strain amplitude (LP #7) having a crack initiation from internal defect, (c) LP specimen under 0.004 mm/mm strain amplitude (LP #6) with a single crack initiation on the surface, and (d) LP specimen under 0.005 mm/mm strain amplitude (LP #4) having multiple crack initiations on the surface.

The microstructure of an as-fabricated without stress relief specimen as well as AB (with stress relief), LP (with prior stress relief), and LPSR (stress relieved before and after LP) specimens were characterized to understand the effect of stress relief and LP. Two different microstructures were observed for each surface condition due to the utilized stress relief thermal process. The SEM images of the microstructure from these four specimens are shown in Fig. 11. As-fabricated specimens before stress relief contained martensitic structures with ultra-fine (<1 μm) acicular features as shown in Fig. 11(a). This could be attributed to the extremely high cooling/solidification rates during the AM process and hence not providing enough time to nucleate the diffusional α phase and develop α laths [10,46,47]. In contrast, the AB specimens after stress relief consisted of acicular + plate-like α structure, as shown in Fig. 11 (b), since these martensitic phases (α') can be decomposed by the reheating process at temperatures in the range of 600–850 °C [48].

To investigate the effect of the LP and secondary stress relief process, the surface was polished ~ 10 μm by a FIB inside of the SEM. Fig. 11(c) and (d) show the microstructure of LP and LPSR specimens, within the laser-treated zone, after the FIB process revealing the LPSR specimens consisted of thicker plate-like α-laths compared to LP specimens. This increase in lath width is a result of the secondary stress relief performed after LP. After secondary stress relief, the laser influenced section decomposed to the plate-like α phase as shown in Fig. 11(d) similar to the as-fabricated specimen after stress relief.

LP irradiated sufficient energy only on the specific area of the surface, and hence, the irradiated spot had a very high temperature with a very high cooling rate. The peak temperature of the irradiated spot was higher than β-transus temperature (994 °C) which, combined with the high cooling rate, resulted in the perpendicular prior β grains and ultra-fine (<1 μm) acicular α' microstructure again close to surface, as shown

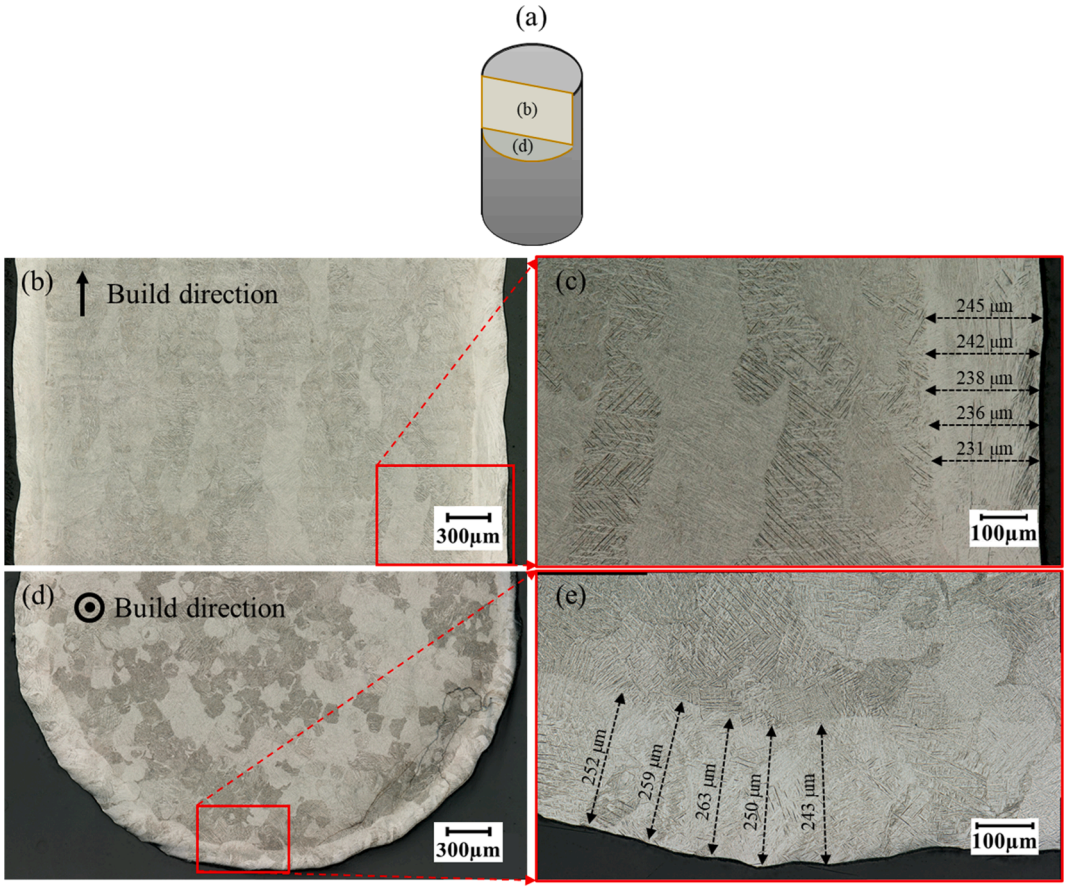

Fig. 10. Optical microscopy images showing (a) schematic describing longitudinal and cross-sectional planes. The polished and chemically etched areas of an LP specimen showing (b) the entire longitudinal area, (c) zoomed-in longitudinal area with thickness measurements, (d) entire cross-sectional area, and (e) zoomed-in cross-sectional area with thickness measurements. Image (c) describes the affected region by a single laser scan and image (e) displays the effective thickness of the LP affected zone caused by multiple laser scans.

in Fig. 11(c) for an area close to the surface. However, the LP does not affect the interior part of the specimen, further away from the surface, and internal sections maintain the acicular + plate-like α structure (similar to the ones in Fig. 11(b)). Tian et al. [30] thoroughly characterized the microstructure of EBM Ti-6Al-4V after LP using EBSD, backscattered images, and TEM. Similar to observations made in this study, they showed that exceptionally fine α + β structure is found in the laser melted region as a thin layer of β between the α lath boundaries.

By considering the solidification of Ti-6Al-4V [49], the retransformed prior β grains close to the surface region had different grain orientations compared to the interior since the solidification direction was perpendicular to the build direction during LB-PBF process. Fig. 12 (a) shows the etched longitudinal surface of LP specimen detailing the reconstructed prior β grain boundaries at the surface. The grain orientation of the internal part is along the build direction, in contrast, the laser influenced region close to the surface shows a distinct orientation identifiable as the dark region at the specimen edge. Since the direction of LP was perpendicular to the build orientation, the direction of the thermal gradient was also perpendicular to the build direction. Therefore, the laser influenced region produces columnar prior β grains irregular in shape (somehow horizontal) to the build direction as shown in Fig. 12(b). The columnar prior β grains regenerated by LP along the transverse direction of the build orientation may affect the cyclic behavior by subjecting the long prior β grains interfaces to tensile opening stresses [50]. However, the effect of microstructure in terms of LP on fatigue strength may be insignificant since the perpendicular grains only regenerated in the solidified region by LP.

According to the SEM images, shown in Fig. 11, LP generated a martensitic microstructure no matter what the previous microstructure was, and it could be decomposed to α by a stress relief process. While it is evident that the martensitic microstructure decomposed during stress relief for the LPSR specimens, it is not clear if this had a greater effect than relieving the residual stress developed during the LP process. To fully decouple these mechanisms more directed studies are needed, however, this work shows that LP not only reconstructs surface topography, but also retransforms the microstructure through fully remelting the surface using highly concentrated energy. As discovered in this section, LP generates enough high temperature to completely remelt and recrystallize the microstructure in the vicinity of the surface. As a result, the effect of stress relief after the AM process vanishes and some of the advantages of the surface polishing becomes null due to the generation of residual stresses in the parts. The secondary stress relief after the LP process can remove the residual stresses, and improve fatigue behavior significantly, even up to the ones from with M/P surfaces.

4. Conclusions

This study investigated the effects of laser polishing, with and without the stress relief process, on the fatigue behavior of LB-PBF Ti-6Al-4V parts. In accordance with the experimental observations of

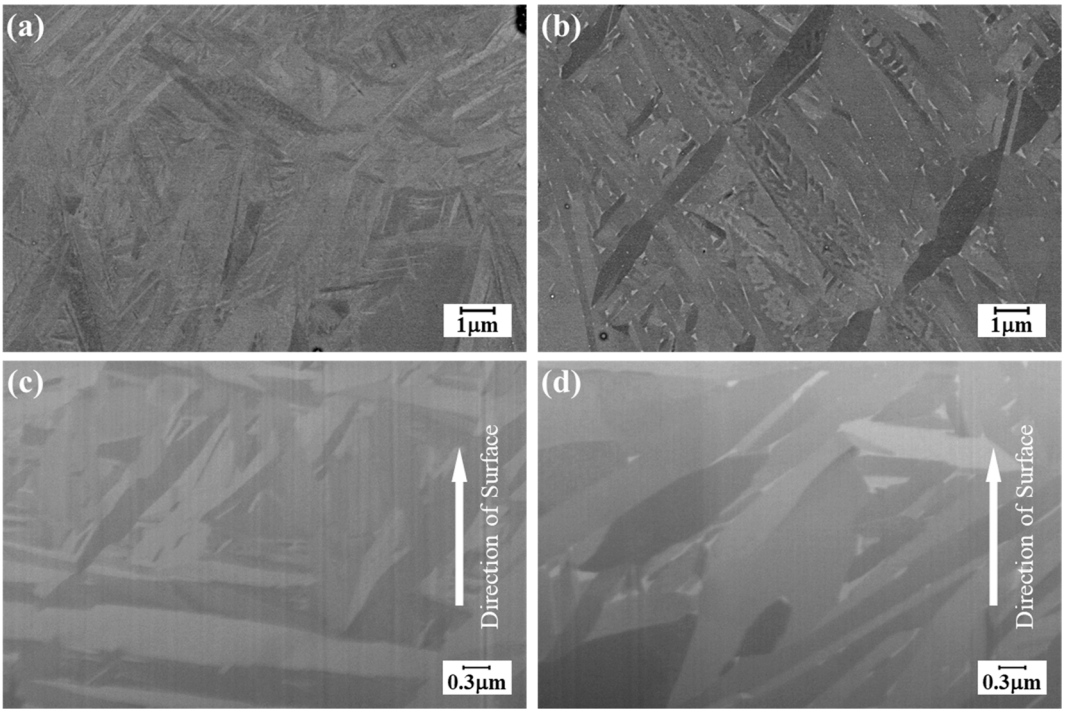

Fig. 11. SEM images showing (a) as-fabricated material before stress relief, and (b) as-fabricated material after stress relief. SEM images after FIB showing (c) LP material before stress relief (the region close to the surface of a LP specimen), and (d) LP material after stress relief (the region close to the surface of a LPSR specimen). The stress relief process transformed the microstructures from (a) to (b) and from (c) to (d).

surface topography, microstructure characterizations, fatigue testing, and fractography, the following conclusions can be made:

1. Laser polishing successfully re-melted partially melted powder particles on the surface of LB-PBF Ti-6Al-4V specimens, since the effective depth of laser polishing was larger than the maximum peak-to-valley depth of the profiled line (R_z). Moreover, the laser polishing reconstructed the surface topography, and hence, the sharpness of the surface profile became smoother.
2. The high cycle fatigue strength of laser polished specimens was improved as compared to specimens with as-built surfaces. However, in the low cycle fatigue regime, laser polished specimens had lower fatigue strengths compared to specimens with as-built surfaces. The increase in high cycle fatigue resistance for laser polished specimens was related to the lower surface roughness, while their lower low cycle fatigue resistance was attributed to residual stresses generated by the laser polishing.
3. Stress relieved laser polished specimens showed improved fatigue resistance for both low and high cycle fatigue regimes than both specimens with as-built surfaces and laser polished specimens without the secondary stress relief. In some cases, the fatigue lives of laser polished specimens with the secondary stress relief were similar to the ones of machined/polished specimens.
4. Laser polishing resulted in grain boundary grooves on the surface which align with the prior β grain boundaries. These grain boundary grooves do not affect the fatigue strength since depths are less than ~ 1 μm and are not as detrimental as process-induced defects such as surface roughness and pores.
5. The microstructure of LB-PBF Ti-6Al-4V was decomposed by the stress relief process; however, laser polishing retransformed microstructure close to the surface into martensitic structures. After secondary stress relief, the laser influenced zone was again decomposed to the plate-like α phase.

These outcomes emphasize that laser polishing can be an attractive post-processing method for additive manufactured components in fatigue critical applications. The detrimental surface roughness can be reconstructed without wasting materials, contrary to some other post-processing methods. Furthermore, the flexibility of laser polishing enables more precise post-processing of complex geometries such as curved structures and bone implants.

CRediT authorship contribution statement

Seungjong Lee: Conceptualization, Methodology, Validation, Formal analysis, Investigation, Data curation, Writing - original draft, Visualization. **Zabihollah Ahmadi:** Conceptualization, Methodology, Validation, Investigation, Writing - original draft. **Jonathan W. Pegues:** Validation, Formal analysis, Data curation, Writing - review & editing. **Masoud Mahjouri-Samani:** Conceptualization, Methodology, Resources, Formal analysis, Investigation, Writing - review & editing, Supervision, Project administration. **Nima Shamsaei:** Conceptualization, Methodology, Resources, Formal analysis, Investigation, Writing - review & editing, Supervision, Project administration, Funding acquisition.

Declaration of Competing Interest

None.

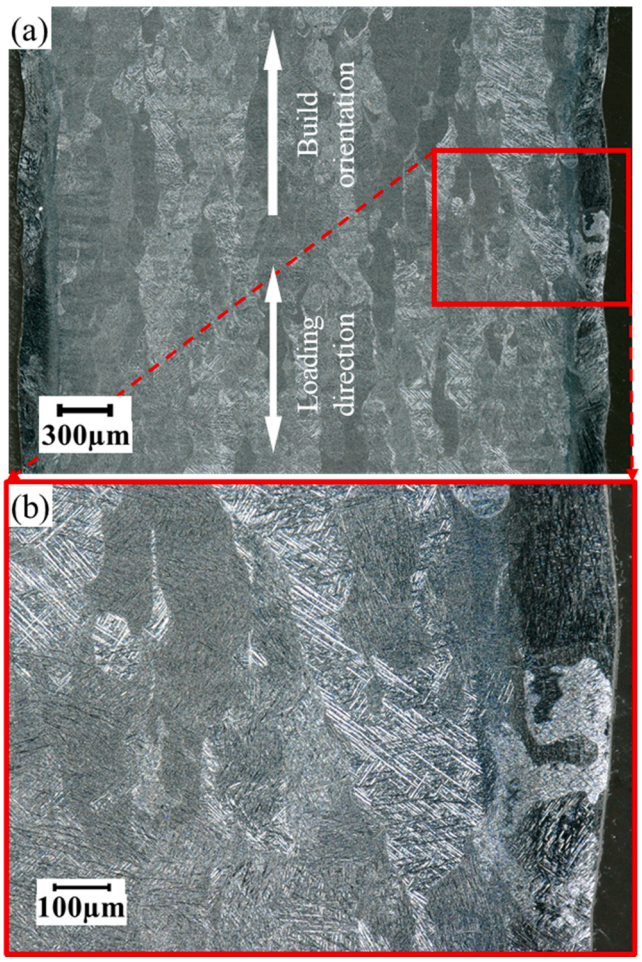

Fig. 12. Longitudinal-section of the LP specimen with build orientation and loading direction indicated. (a) Grain orientations of the entire region, and (b) columnar grains close to the surface deviating from the build orientation/loading direction.

Acknowledgments

Sandia National Laboratories is a multimission laboratory managed and operated by National Technology and Engineering Solutions of Sandia LLC, a wholly owned subsidiary of Honeywell International Inc. for the U.S. Department of Energy's National Nuclear Security Administration under contract DE-NA0003525. This paper describes objective technical results and analysis. Any subjective views or opinions that might be expressed in the paper do not necessarily represent the views of the U.S. Department of Energy or the United States Government.

References

[1] W.E. Frazier, Metal additive manufacturing: A review, J. Mater. Eng. Perform. 23 (2014) 1917–1928, https://doi.org/10.1007/s11665-014-0958-z.
[2] M. Leary, M. Mazur, M. Watson, E. Boileau, M. Brandt, Voxel-based support structures for additive manufacture of topologically optimal geometries, Int. J. Adv. Manuf. Technol. 105 (2019) 1–26, https://doi.org/10.1007/s00170-019-03964-z.
[3] A. Yadollahi, N. Shamsaei, Additive manufacturing of fatigue resistant materials: Challenges and opportunities, Int. J. Fatigue. 98 (2017) 14–31, https://doi.org/10.1016/j.ijfatigue.2017.01.001.
[4] N. Shamsaei, A. Yadollahi, L. Bian, S.M. Thompson, An overview of Direct Laser Deposition for additive manufacturing; Part II: Mechanical behavior, process parameter optimization and control, Addit. Manuf. 8 (2015) 12–35, https://doi.org/10.1016/j.addma.2015.07.002.
[5] X. Wang, S. Xu, S. Zhou, W. Xu, M. Leary, P. Choong, M. Qian, M. Brandt, Y.M. Xie, Topological design and additive manufacturing of porous metals for bone scaffolds and orthopaedic implants: A review, Biomaterials. 83 (2016) 127–141, https://doi.org/10.1016/j.biomaterials.2016.01.012.
[6] R. Huang, M. Riddle, D. Graziano, J. Warren, S. Das, S. Nimbalkar, J. Cresko, E. Masanet, Energy and emissions saving potential of additive manufacturing: the case of lightweight aircraft components, J. Clean. Prod. 135 (2016) 1559–1570, https://doi.org/10.1016/j.jclepro.2015.04.109.
[7] G. Bi, A. Gasser, Restoration of nickel-base turbine blade knife-edges with controlled laser aided additive manufacturing, Phys. Proc. (2011) 402–409, https://doi.org/10.1016/j.phpro.2011.03.051.
[8] A.M. Beese, B.E. Carroll, Review of Mechanical Properties of Ti-6Al-4V Made by Laser-Based Additive Manufacturing Using Powder Feedstock, JOM. 68 (2016) 724–734, https://doi.org/10.1007/s11837-015-1759-z.
[9] M. Qian, W. Xu, M. Brandt, H.P. Tang, Additive manufacturing and postprocessing of Ti-6Al-4V for superior mechanical properties, MRS Bull. 41 (2016) 775–783, https://doi.org/10.1557/mrs.2016.215.
[10] J.W. Pegues, S. Shao, N. Shamsaei, N. Sanaei, A. Fatemi, D.H. Warner, P. Li, N. Phan, Fatigue of additive manufactured Ti-6Al-4V, Part I: The effects of powder feedstock, manufacturing, and post-process conditions on the resulting microstructure and defects, Int. J. Fatigue. 132 (2020), 105358, https://doi.org/10.1016/j.ijfatigue.2019.105358.
[11] R. Molaei, A. Fatemi, N. Sanaei, J. Pegues, N. Shamsaei, S. Shao, P. Li, D.H. Warner, N. Phan, Fatigue of additive manufactured Ti-6Al-4V, Part II: The relationship between microstructure, material cyclic properties, and component performance, Int. J. Fatigue. 132 (2020), 105363, https://doi.org/10.1016/j.ijfatigue.2019.105363.
[12] A. Fatemi, R. Molaei, J. Simsiriwong, N. Sanaei, J. Pegues, B. Torries, N. Phan, N. Shamsaei, Fatigue behaviour of additive manufactured materials: An overview of some recent experimental studies on Ti-6Al-4V considering various processing and loading direction effects, Fatigue Fract. Eng. Mater. Struct. 42 (2019) 991–1009, https://doi.org/10.1111/ffe.13000.
[13] M.V. Ribeiro, M.R.V. Moreira, J.R. Ferreira, Optimization of titanium alloy (6Al-4V) machining, in, J. Mater. Process. Technol. (2003) 458–463, https://doi.org/10.1016/S0924-0136(03)00457-6.
[14] M.J. Bermingham, J. Kirsch, S. Sun, S. Palanisamy, M.S. Dargusch, New observations on tool life, cutting forces and chip morphology in cryogenic machining Ti-6Al-4V, Int. J. Mach. Tools Manuf. 51 (2011) 500–511, https://doi.org/10.1016/j.ijmachtools.2011.02.009.
[15] M. Kahlin, H. Ansell, D. Basu, A. Kerwin, L. Newton, J.J. Moverare, Improved fatigue strength of additively manufactured Ti6Al4V by surface post processing, Int. J. Fatigue. 134 (2020), 105497, https://doi.org/10.1016/j.ijfatigue.2020.105497.
[16] G. Strano, L. Hao, R.M. Everson, K.E. Evans, Surface roughness analysis, modelling and prediction in selective laser melting, J. Mater. Process. Technol. 213 (2013) 589–597, https://doi.org/10.1016/j.jmatprotec.2012.11.011.
[17] J. Kranz, D. Herzog, C. Emmelmann, Design guidelines for laser additive manufacturing of lightweight structures in TiAl6V4, J. Laser Appl. 27 (2015) S14001, https://doi.org/10.2351/1.4885235.
[18] M. Taufik, P.K. Jain, Role of build orientation in layered manufacturing: A review, Int. J. Manuf. Technol. Manag. 27 (2013) 47–73, https://doi.org/10.1504/IJMTM.2013.058637.
[19] J. Gockel, L. Sheridan, B. Koerper, B. Whip, The influence of additive manufacturing processing parameters on surface roughness and fatigue life, Int. J. Fatigue. 124 (2019) 380–388, https://doi.org/10.1016/j.ijfatigue.2019.03.025.
[20] A. Triantaphyllou, C.L. Giusca, G.D. Macaulay, F. Roerig, M. Hoebel, R.K. Leach, B. Tomita, K.A. Milne, Surface texture measurement for additive manufacturing, Surf. Topogr. Metrol. Prop. 3 (2015) 1–8, https://doi.org/10.1088/2051-672X/3/2/024002.
[21] J.W. Pegues, N. Shamsaei, M.D. Roach, R.S. Williamson, Fatigue life estimation of additive manufactured parts in the as-built surface condition, Mater. Des. Process. Commun. 1 (2019), e36, https://doi.org/10.1002/mdp2.36.
[22] J. Zhang, A. Fatemi, Surface roughness effect on multiaxial fatigue behavior of additive manufactured metals and its modeling, Theor. Appl. Fract. Mech. 103 (2019), 102260, https://doi.org/10.1016/j.tafmec.2019.102260.
[23] F.E. Pfefferkorn, N.A. Duffie, J.D. Morrow, Q. Wang, Effect of beam diameter on pulsed laser polishing of S7 tool steel, CIRP Ann. - Manuf. Technol. 63 (2014) 237–240, https://doi.org/10.1016/j.cirp.2014.03.055.
[24] E. Ukar, A. Lamikiz, F. Liébana, S. Martínez, I. Tabernero, An industrial approach of laser polishing with different laser sources: Industrielle Methode zum Laserpolieren mit verschiedenen Laserstrahlquellen, Materwiss. Werksttech. 46 (2015) 661–667, https://doi.org/10.1002/mawe.201500324.
[25] Q. Wang, J.D. Morrow, C. Ma, N.A. Duffie, F.E. Pfefferkorn, Surface prediction model for thermocapillary regime pulsed laser micro polishing of metals, J. Manuf. Process. 20 (2015) 340–348, https://doi.org/10.1016/j.jmapro.2015.05.005.
[26] W. Zhang, K. Wong, M. Morales, C. Molpeceres, C. Arnold, Implications of Using Two Low-power Continuous-wave Lasers for Polishing, Int. J. Extrem. Manuf. (2020), https://doi.org/10.1088/2631-7990/ab94c6.
[27] L. Zhao, J. Cheng, M. Chen, X. Yuan, W. Liao, Q. Liu, H. Yang, H. Wang, Formation mechanism of a smooth, defect-free surface of fused silica optics using rapid CO 2 laser polishing, Int. J. Extrem. Manuf. 1 (2019), 035001, https://doi.org/10.1088/2631-7990/ab3033.
[28] W. Guo, M. Hua, P.W.T. Tse, A.C.K. Mok, Process parameters selection for laser polishing DF2 (AISI O1) by Nd:YAG pulsed laser using orthogonal design, Int. J. Adv. Manuf. Technol. 59 (2012) 1009–1023, https://doi.org/10.1007/s00170-011-3558-1.
[29] L. Giorleo, E. Ceretti, C. Giardini, Ti surface laser polishing: Effect of laser path and assist gas, Proc. CIRP (2015) 446–451, https://doi.org/10.1016/j.procir.2015.06.102.

[30] Y. Tian, W.S. Gora, A.P. Cabo, L.L. Parimi, D.P. Hand, S. Tammas-Williams, P. B. Prangnell, Material interactions in laser polishing powder bed additive manufactured Ti6Al4V components, Addit. Manuf. 20 (2018) 11–22, https://doi.org/10.1016/j.addma.2017.12.010.
[31] C. Liang, Y. Hu, N. Liu, X. Zou, H. Wang, X. Zhang, Y. Fu, J. Hu, Laser polishing of Ti6Al4V fabricated by selective laser melting, Metals (Basel). 10 (2020) 1–13, https://doi.org/10.3390/met10020191.
[32] P.E. Carrion, A. Soltani-Tehrani, N. Phan, N. Shamsaei, Powder Recycling Effects on the Tensile and Fatigue Behavior of Additively Manufactured Ti-6Al-4V Parts, Jom. 71 (2019) 963–973, https://doi.org/10.1007/s11837-018-3248-7.
[33] International Organization for Standardization, ISO 4287:1997. Geometrical product specifications (GPS). Surface texture: profile method. Terms, definitions and surface texture parameters, Geneva, 1997.
[34] J. Pegues, M. Roach, R. Scott Williamson, N. Shamsaei, Surface roughness effects on the fatigue strength of additively manufactured Ti-6Al-4V, Int. J. Fatigue. 116 (2018) 543–552, https://doi.org/10.1016/j.ijfatigue.2018.07.013.
[35] A. Gursel, Crack risk in Nd: YAG laser welding of Ti-6Al-4V alloy, Mater. Lett. 197 (2017) 233–235, https://doi.org/10.1016/j.matlet.2016.12.112.
[36] E. Akman, A. Demir, T. Canel, T. Sinmazçelik, Laser welding of Ti6Al4V titanium alloys, J. Mater. Process. Technol. 209 (2009) 3705–3713, https://doi.org/10.1016/j.jmatprotec.2008.08.026.
[37] K.S. Chan, Characterization and analysis of surface notches on Ti-alloy plates fabricated by additive manufacturing techniques, Surf. Topogr. Metrol. Prop. 3 (2015), 044006, https://doi.org/10.1088/2051-672X/3/4/044006.
[38] P. Tyagi, T. Goulet, C. Riso, R. Stephenson, N. Chuenprateep, J. Schlitzer, C. Benton, F. Garcia-Moreno, Reducing the roughness of internal surface of an additive manufacturing produced 316 steel component by chempolishing and electropolishing, Addit. Manuf. 25 (2019) 32–38, https://doi.org/10.1016/j.addma.2018.11.001.
[39] B. Vayssette, N. Saintier, C. Brugger, M. Elmay, E. Pessard, Surface roughness of Ti-6Al-4V parts obtained by SLM and EBM: Effect on the High Cycle Fatigue life, Proc. Eng. 213 (2018) 89–97, https://doi.org/10.1016/j.proeng.2018.02.010.
[40] V. Chastand, P. Quaegebeur, W. Maia, E. Charkaluk, Comparative study of fatigue properties of Ti-6Al-4V specimens built by electron beam melting (EBM) and selective laser melting (SLM), Mater. Charact. 143 (2018) 76–81, https://doi.org/10.1016/j.matchar.2018.03.028.
[41] R.I. Stephens, A. Fatemi, R.R. Stephens, H.O. Fuchs, Metal fatigue in engineering, 2nd ed., John Wiley & Sons, 2000.
[42] H. Masuo, Y. Tanaka, S. Morokoshi, H. Yagura, T. Uchida, Y. Yamamoto, Y. Murakami, Influence of defects, surface roughness and HIP on the fatigue strength of Ti-6Al-4V manufactured by additive manufacturing, Int. J. Fatigue. 117 (2018) 163–179, https://doi.org/10.1016/j.ijfatigue.2018.07.020.
[43] D. Greitemeier, C. Dalle Donne, F. Syassen, J. Eufinger, T. Melz, Effect of surface roughness on fatigue performance of additive manufactured Ti–6Al–4V, Mater. Sci. Technol. 32 (2016) 629–634, https://doi.org/10.1179/1743284715Y.0000000053.
[44] D. Greitemeier, F. Palm, F. Syassen, T. Melz, Fatigue performance of additive manufactured TiAl6V4 using electron and laser beam melting, Int. J. Fatigue. 94 (2017) 211–217, https://doi.org/10.1016/j.ijfatigue.2016.05.001.
[45] S. Lee, J. Pegues, N. Shamsaei, Fatigue Behavior and Modeling for Additive Manufactured 304L Stainless Steel: The effect of Surface Roughness, Int. J. Fatigue. 141 (2020), 105856, https://doi.org/10.1016/j.ijfatigue.2020.105856.
[46] W. Xu, M. Brandt, S. Sun, J. Elambasseril, Q. Liu, K. Latham, K. Xia, M. Qian, Additive manufacturing of strong and ductile Ti-6Al-4V by selective laser melting via in situ martensite decomposition, Acta Mater. 85 (2015) 74–84, https://doi.org/10.1016/j.actamat.2014.11.028.
[47] D.K. Do, P. Li, The effect of laser energy input on the microstructure, physical and mechanical properties of Ti-6Al-4V alloys by selective laser melting, Virtual Phys. Prototyp. 11 (2016) 41–47, https://doi.org/10.1080/17452759.2016.1142215.
[48] W. Xu, E.W. Lui, A. Pateras, M. Qian, M. Brandt, In situ tailoring microstructure in additively manufactured Ti-6Al-4V for superior mechanical performance, Acta Mater. 125 (2017) 390–400, https://doi.org/10.1016/j.actamat.2016.12.027.
[49] P.A. Kobryn, S.L. Semiatin, Microstructure and texture evolution during solidification processing of Ti-6A1-4V, J. Mater. Process. Technol. 135 (2003) 330–339, https://doi.org/10.1016/S0924-0136(02)00865-8.
[50] B.E. Carroll, T.A. Palmer, A.M. Beese, Anisotropic tensile behavior of Ti-6Al-4V components fabricated with directed energy deposition additive manufacturing, Acta Mater. (2015), https://doi.org/10.1016/j.actamat.2014.12.054.